Seasonal stratification of the upper ocean salinity stratification in the Tropics

C. Maes, T. O'Kane

AGU PUBLICATIONS

JGR

Journal of Geophysical Research: Oceans

RESEARCH ARTICLE

10.1002/2013JC009366

Key Points:
- Describe ocean salinity stratification (OSS)
- Describe its seasonal variations
- Relate the OSS to the surface SST and SSS fields

Supporting Information:
- Readme file
- Figure S1–S4

Correspondence to:
C. Maes,
Christophe.Maes@ird.fr

Citation:
Maes, C., and T. J. O'Kane (2014), Seasonal variations of the upper ocean salinity stratification in the Tropics, *J. Geophys. Res. Oceans*, *119*, 1706–1722, doi:10.1002/2013JC009366.

Received 21 AUG 2013
Accepted 16 JAN 2014
Accepted article online 22 JAN 2014
Published online 10 MAR 2014

Seasonal variations of the upper ocean salinity stratification in the Tropics

Christophe Maes[1] and Terence J. O'Kane[2,3]

[1]IRD, LEGOS, UMR Université Paul Sabatier/IRD/CNRS/CNES, Toulouse, France, [2]CSIRO Marine and Atmospheric Research, Hobart, Tasmania, Australia, [3]Center for Australian Weather and Climate Research, Melbourne, Victoria, Australia

Abstract In comparison to the deep ocean, the upper mixed layer is a region typically characterized by substantial vertical gradients in water properties. Within the Tropics, the rich variability in the vertical shapes and forms that these structures can assume through variation in the atmospheric forcing results in a differential effect in terms of the temperature and salinity stratification. Rather than focusing on the strong halocline above the thermocline, commonly referred to as the salinity barrier layer, the present study takes into account the respective thermal and saline dependencies in the Brunt-Väisälä frequency (N^2) in order to isolate the specific role of the salinity stratification in the layers above the main pycnocline. We examine daily vertical profiles of temperature and salinity from an ocean reanalysis over the period 2001–2007. We find significant seasonal variations in the Brunt-Väisälä frequency profiles are limited to the upper 300 m depth. Based on this, we determine the ocean salinity stratification (OSS) to be defined as the stabilizing effect (positive values) due to the haline part of N^2 averaged over the upper 300 m. In many regions of the tropics, the OSS contributes 40–50% to N^2 as compared to the thermal stratification and, in some specific regions, exceeds it for a few months of the seasonal cycle. Away from the tropics, for example, near the centers of action of the subtropical gyres, there are regions characterized by the permanent absence of OSS. In other regions previously characterized with salinity barrier layers, the OSS obviously shares some common variations; however, we show that where temperature and salinity are mixed over the same depth, the salinity stratification can be significant. In addition, relationships between the OSS and the sea surface salinity are shown to be well defined and quasilinear in the tropics, providing some indication that in the future, analyses that consider both satellite surface salinity measurements at the surface and vertical profiles at depth will result in a better determination of the role of the salinity stratification in climate prediction systems.

1. Introduction

The conceptual view of the ocean vertical structure is based on the definition of several layers where the properties of the water parcels exhibit different levels of vertical uniformity. At the surface, turbulence generated by the wind and buoyancy fluxes creates a layer through active vertical mixing and energy dissipation. This mixed layer occurs because of temporal variations in turbulence intensity and is defined as the upper portion of the surface layer where the temperature and salinity, and thus density, are well mixed and exhibit a vertically uniform structure characterized by a uniform density profile. The depth over which such mixing processes occurs is ultimately determined by the balance between the destabilizing effects of mechanical input and the stabilizing effects of the surface buoyancy. Below the mixed layer depth (MLD), stratification occurs and results in the presence of the seasonal and permanent pycnocline, i.e., where the vertical density gradients are maximum. In temperature, this highly stratified zone is referred to as the thermocline, and in the case of salinity it is called the halocline. The base of the main pycnocline marks the depth limit of the upper ocean surface layer.

In the absence of direct turbulent dissipation measurements, the different depths of the upper ocean layers are commonly derived from profile data using threshold or other proxy variables. The different methodologies often yield different values for the MLD depending on the source of data and definition used for the upper ocean features [e.g., *Thomson and Fine*, 2003]. In the Tropics, another level of complexity in the vertical structure of the surface layer was revealed by large differences between the bases of the thermocline and halocline in the western equatorial Pacific [*Lukas and Lindstrom*, 1991]. This phenomenon is not only

relevant to the western equatorial Pacific region but is common over the entire tropical band [*Sprintall and Tomczak*, 1992]. It has been recognized that salinity stratification exerts an important influence on the mixed layer dynamics and heat budget, thus layers where significant differences between the thermocline/halocline base exist have been named the salinity barrier layer thickness (BLT).

Various studies have examined BLT phenomena in the tropical oceans. *de Boyer Montégut et al*. [2007] presented a general description of BLT seasonal climatology based on the individual analysis of instantaneous profiles. Moreover, *Maes et al*. [2002, 2005] and *Maes and Belamari* [2011] showed the variability of the BLT to be crucial for understanding the response of the coupled air-sea interactions involved in the El Niño/Southern Oscillation (ENSO) phenomenon. In their sensitivity experiments, the effect of the BLT was removed through the explicit cancelation of the salinity stratification in the computation of the Brunt Väisälä frequency (i.e., the salinity remained free to vary in perturbed experiments). They showed that in regions where BLT formation was suppressed, rather than finding a systematic and expected cooling effect on the sea surface temperature (SST), there occurred instead a substantial deepening of the mixed layer depth. This result suggests that the control of the mixing conditions in the upper oceanic layers depends critically on the general features of salinity stratification above the main pycnocline.

In this study, we propose a new perspective and methodology for describing the impact of the salinity on the static stratification of the oceanic upper layers. This perspective recognizes that the stabilizing effect of the salinity operates near the bottom of the mixed layer but that its effect could be expanded down to the main pycnocline and to regions where both the salinity and temperature are mixed over the same depths. Here we consider a methodology that treats the salinity stratification in a simple partitioning of the thermal and haline effects in the vertical profiles of $N^2(T, S)$, the Brunt Väisälä frequency, in the manner advocated by *McDougall* [1987]. This approach, which is constrained by neither thresholds nor a priori limits for determining the different layers of the ocean such as the mixed layer, results in physically interpretable patterns while avoiding the disadvantages of commonly used methods associated with the barrier layer formalism. This framework further allows us to connect the surface fields of sea surface salinity (SSS) and SST to changes in the stratification of the upper layers above the main pycnocline in the oceans.

The remainder of the paper is organized as follows. Section 2 provides a description of the reanalyzed vertical profiles of temperature and salinity used as the data source, and the formal definition of the ocean salinity stratification (OSS). Section 3 presents the results, which include the main patterns of the seasonal cycle of the OSS in the Tropics (30°N–30°S). The paper concludes with discussion and conclusions in the sections 4 and 5.

2. Ocean Model Data and Methodology

2.1. The Ocean Model Configuration

Our model is based on the Australian Community Climate Earth System Simulator-Ocean (ACCESS-O) configuration of the GFDL MOM4p1 ocean-ice code [*Delworth et al*., 2006]. A volume conserving approach based on the Boussinesq z^* coordinates scaled with height along the vertical is used. The horizontal resolution is nominally 1° with equatorial refinement to 1/3° in the tropical band between 10°S and 10°N and a Mercator (cosine dependent) implementation for the Southern Hemisphere applied, ranging from 1/4° at 78°S to 1° at 30°S. In the vertical, ACCESS-O implements the z^* coordinate available in MOM4p1, with 50 model levels covering 0–6000 m with a resolution ranging from 10 m in the upper layers (0–200 m) to about 333 m for the abyssal ocean. A detailed description of the model and physics can be found in *O'Kane et al*. [2013a].

The model reanalyzes described in this study employ atmospheric fields from the CORE.v2 (hereafter CORE2) interannually varying forcing [*Griffies et al*., 2009; *Large and Yeager*, 2009]. In addition, a weak restoring is applied to the surface salinity of the top layer (equivalent thickness of 10 m) that is relaxed to World Ocean Atlas (WOA09) fields with a time scale of 60 days in order to reduce drift [*O'Kane et al*., 2013a]. The model is further constrained by relaxing the ocean temperature and salinity at depths below 2000 m to WOA09 climatology with a 1 year relaxation time scale. The model spin-up for the reanalysis consists of a 60 year control integration using CORE2 forcing with atmospheric fields that are converted to air-sea fluxes with bulk formulas. Precipitation minus evaporation (P-E) fluxes are similarly adjusted consistently relative to the CORE2 forcing. The initial conditions for temperature and salinity fields come from WOA09 climatology.

2.2. Ocean Data Assimilation

The model is integrated with a modified variant of the BODAS ensemble optimal interpolation (EnOI) data assimilation system to produce an ocean reanalysis for the period 1990–2008 [*Oke et al*., 2008, 2013]. The EnOI method employs background error covariances defined from a stationary, or time invariant, ensemble of seasonal anomalies (432 monthly mean anomaly ensemble members) derived from the last 36 years of the control model integration. A series of global reanalyses were conducted as part of an observing system experiment (OSE) to quantify the relative impact of subsurface, satellite, and altimetric data. Here we use a 14 day window of observations and a 14 day update cycle for reanalyses that include only temperature and salinity profile observations from eXpendable BathyThermograph (XBT), Conductivity-Temperature-Depth (CTD) and Argo and satellite SST. Background error covariances are localized according to the Shur product method of *Gaspari and Cohn* [1999]. As both our model and observational spatial resolution are of the order of 1°, we employ a localization length scale of 8°. Analysis updates are introduced gradually into the model integration to ensure consistency with the background innovations and reduce model shock [*Bloom et al*., 1996]. A major advantage of EnOI is that the background error covariances are inhomogeneous and anisotropic and therefore better reflect the variability and length scales of the ocean circulation [*Oke et al*., 2008]. At each update step, the adaptive initialization scheme of *Sandery et al*. [2011] is employed, ensuring more balanced initial conditions than is possible using Newtonian relaxation. The updated variables are temperature, salinity, and surface height.

Prior to January 1998, in situ profiles of temperature and salinity are assimilated from hydrographic data from World Ocean Circulation Experiment (WOCE) Hydrographic Program (WHP), World Ocean Database 2005 (WOD05) [*Boyer et al*., 2006], and the Quality controlled Ocean Temperature Archive (QuOTA) [*Gronell and Wijffels*, 2008], which contains all XBT data in the Indian and South-West Pacific. After January 1998, we assimilate the WOCE Upper Ocean Thermal (UOT) database that includes global XBT data, except in the Indian Ocean where we use QuOTA for XBTs. Temperature and salinity are assimilated from Argo profiles and from the Tropical Atmosphere Ocean (TAO) array [*Oke et al*., 2013].

Standard deviations of T and S analysis increments (supporting information Figure S1) averaged over the upper 350 m are largest in the western boundary current regions. This is to be expected as our model is not eddy resolving and our assimilation system (background covariances) is configured to resolve monthly time scales. In the equatorial region, standard deviations of the increments are ∼0.5°C for T and less than 0.1 psu for salinity. The standard deviations at each depth averaged over ±20° of latitude (supporting information Figure S2) reveal the largest background (forecast) errors occur in the thermocline for temperature and in the surface of the western Pacific, eastern Indian, and western Atlantic for salinity. The thermocline and mixed layers where the Amazon River discharges (∼50°W), the Arabian Sea and the Bay of Bengal are the other major regions of large errors. From the analysis innovations (ai), we see that the assimilation typically fits T to within ∼0.5°C and S to within 0.2 psu in the upper 300 m (supporting information Figure S3). The background innovations in the Pacific averaged over ±30° latitude (supporting information Figure S3) show that the largest background errors at 2 weeks lead time occur about the thermocline. The standard deviations of the background errors dramatically decrease over the period 2001–2004 as progressively more vertical profiles from the Argo data set become available for assimilation and the model upper ocean is constrained. For salinity, the background innovations show largest errors at the surface and at about 200 m with some evidence of a seasonal effect. Analysis innovations show the fit to the observations. For SST (supporting information Figure S4), there is a marked reduction in both the analysis and background innovation errors of ∼0.3°C in 2002 indicating the impact of SST data from the AMSR-E radiometer (supporting information Figure S4). Most obviously, we found that the model thermocline is progressively better constrained as Argo data coverage is increased. Consequently, in the following, we have focused our diagnostics on the period 2001–2007 only.

2.3. Methodology

The stability of the water column can be tested by considering the exchange of two parcels of fluid at different levels. The measure of the degree of stability is given by the Brunt Väisälä frequency, N^2 (also called the stability frequency). In the ocean, N^2 can be expressed in terms of the vertical profiles of temperature and salinity as follows:

$$N^2(T,S) = -\frac{g}{\rho}\frac{\partial \rho}{\partial z} \approx \left(g\alpha\frac{\partial T}{\partial z} - g\beta\frac{\partial S}{\partial z}\right)$$

$$= N^2{}_T(T,S) + N^2{}_S(T,S)$$

where

$$N^2{}_T(T,S) = g\alpha\frac{\partial T}{\partial z}$$

$$N^2{}_S(T,S) = N^2(T,S) - N^2{}_T(T,S)$$

$$\alpha = -\rho^{-1}\frac{\partial \rho}{\partial T}$$

$$\beta = \rho^{-1}\frac{\partial \rho}{\partial S}$$

where β is the haline contraction coefficient, α is the thermal expansion coefficient, g is gravity, ρ is the density, T is the temperature, S is the salinity, and z is the depth. Throughout and for convenience, we will use the abbreviated notation

$$N^2{}_T(T,S) \rightarrow N^2(T), \quad N^2{}_S(T,S) \rightarrow N^2(S)$$

In the following, the ocean salinity stratification (OSS) is defined in terms of the difference between N^2(T, S) and N^2(T) thereby allowing the identification of the layer where the salinity stratification has its greatest impact on buoyancy in terms of stabilizing the water masses [*Maes*, 2008]. Specifically, we define OSS as the vertical mean average of positive N^2(S) over the upper 300 m depth range, i.e.,

$$OSS = \langle N^2(T,S) - N^2(T) \rangle_{0-300\mathrm{m}}$$

where

$$N^2(T,S) - N^2(T) > 0$$

which typically occurs above the maximum of N^2(T, S). Importantly, the OSS measures the strength of the salinity stratification above the main thermocline and is independent of the position of the mixed layer. Where the OSS is negative, salinity has a destabilizing effect and can, where N^2(T) is attenuated, be further associated with regions of density compensation [see *O'Kane et al.*, 2013b, and references therein]. Such regions are to be the subject of a future study.

3. Results

Reanalyzed daily profiles of temperature, salinity, and potential density are used to calculate the Brunt Väisälä frequency and determine the annual mean and seasonal cycle over the period 2001–2007. Figure 1a shows the annual mean depth of the maximum of N^2(T, S) along the water column. This allows one to identify the position of the permanent pycnocline and further determine regions of substantial vertical gradients in water properties. Within the 10°N–10°S band of the Atlantic and Pacific Ocean, the depth patterns of the pycnocline surface are close to the depth of the 20°C isotherm (used as a proxy for the thermocline depth, not shown), revealing the predominance of the thermal effect. At the scale of these basins, the large gradient between the deeper western and shallower eastern thermocline is due to the response to the trade winds. In the Indian Ocean, the mean equatorial structure across the basin is zonally flattened at the scale of the basin, a fact that is also related to the monsoon regime differences in the wind field features. Outside the tropical band, the maximum N^2(T, S) values are reached near the center of the subtropical gyres and in the western boundary currents of the Kuroshio and, to a lesser extent, the Gulf Stream. The absolute largest N^2(T, S) values are found in the southeastern Pacific Ocean, with typical depths of 300 m in the mean. Globally, these features are consistent with our current knowledge of flows within the thermocline and the wind driven circulation.

The vertical structure of the upper ocean is primarily defined by changes in the temperature and salinity fields that together control the water column's density structure. A consequence of this is that the thermocline and the halocline may not always exactly coincide in their depth range. This is also true for their

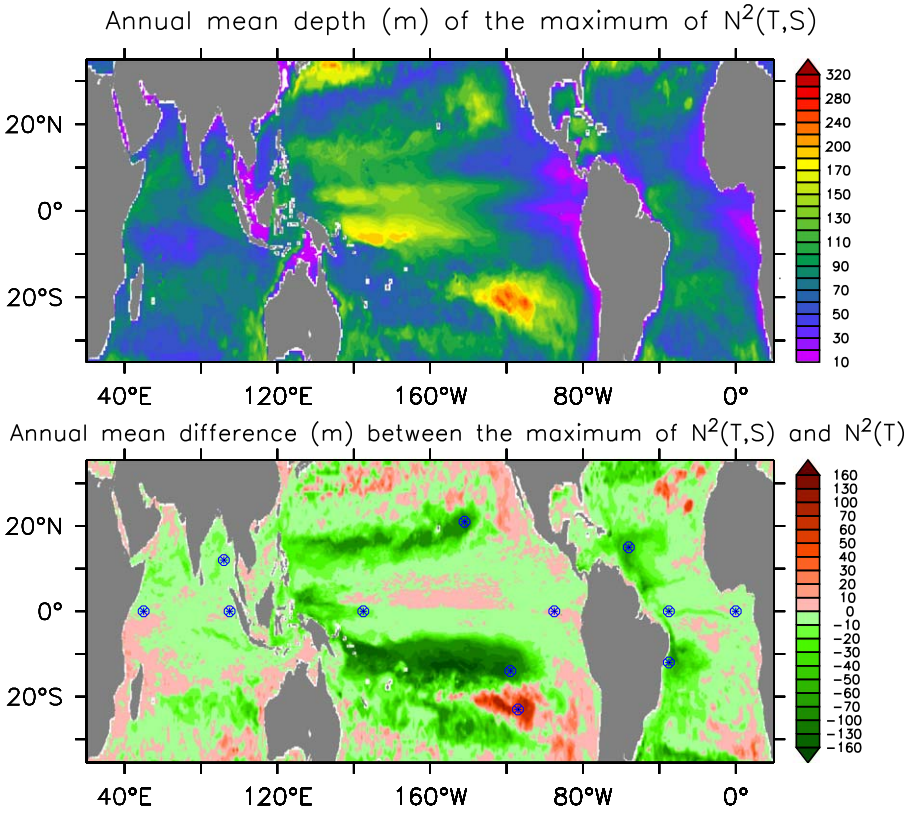

Figure 1. (top) Annual mean depth of the $N^2(T, S)$ maximum in the Tropics and (bottom) annual mean difference between the maximum of $N^2(T, S)$ and $N^2(T)$. Units are in meters. On the bottom, the positions mark the vertical profiles shown in Figures 2 and 3.

relative maxima defined as the mean difference between $N^2(T, S)_{max}$ and $N^2(T)_{max}$ as illustrated in Figure 1b. Differences between the thermocline and halocline are generally around 20–30 m with the main exception being the subtropical gyres and in particular the Pacific Ocean where differences can be larger than 100 m. The large differences in the South Eastern Pacific occur due to the subduction of spiciness (density compensated disturbances) anomalies associated with winter outcropping of the pycnocline [*Kolodziejczyk and Gaillard*, 2013; *O'Kane et al*., 2013b]. For the equatorial regions, to consider only $N^2(T, S)$ masks the fact that the vertical structure of the surface layer in temperature and salinity can be complex and variable, leading to the control of the density structure by one or the other property along the water column. To appreciate the complexity of the forms and thickness of the upper-layer structure, Figures 2 and 3 display vertical profiles of $N^2(T, S)$ and $N^2(T)$ at the different positions indicated in Figure 1b. As expected, the equatorial profiles at 165°E (Figure 2, top left) share large similarities with the profiles observed during the Frontalis cruises and described by *Maes* [2008]. Above the mean pycnocline located around 120 m depth, the values of $N^2(T, S)$ and $N^2(T)$ are very low and close to zero near the surface. Below the mean pycnocline, the values decrease toward a quasiconstant weak but positive value below 300 m depth. The shape of the profile for $N^2(T)$ is similar but characterized by weaker values above the main thermocline/pycnocline. The difference between these two profiles is due to the role of salinity in the static stratification and represents, in essence, the salinity stratification that is the focus of the present study. The main effect of the OSS is to increase the static stratification along this part of the water column.

The profiles displayed in Figure 2 show that the stabilizing effect of salinity within and above the thermocline is not unique to the western Pacific Ocean. Similar differences are found in the eastern Indian Ocean (0°N–95°E, Figure 2, bottom right), and with some smaller amplitude, in the western Atlantic (0°N–35°W, Figure 2, middle left), and the eastern sectors of both Pacific (0°N–165°E, Figure 2, top left) and Atlantic Oceans (0°N–0°W, Figure 2, middle right). In these cases, the most substantial effect of the salinity is located at the level of the pycnocline itself, for example, between 0°N and 95°W or 0°N and 0°W. It is noteworthy to mention that the most important reverse effect representing the destabilizing effect of salinity (i.e., layers

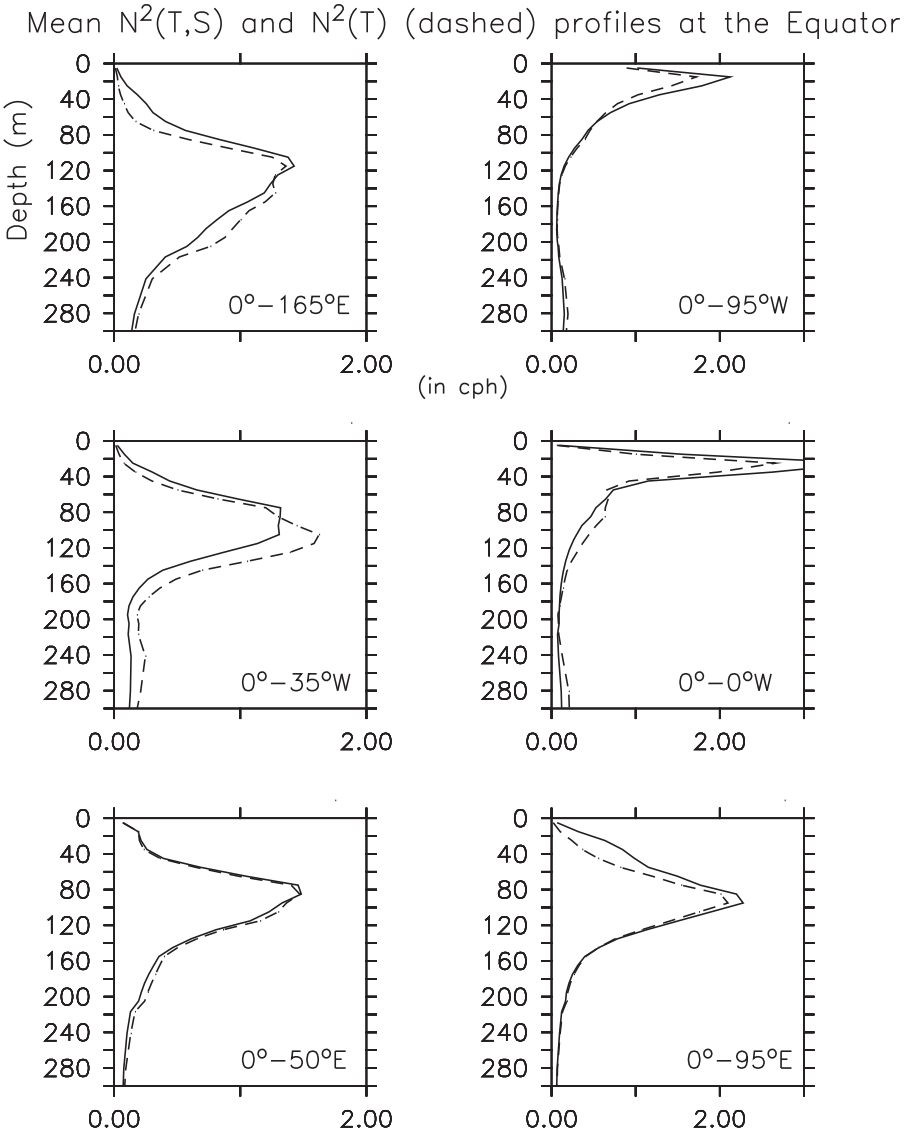

Figure 2. Annual mean profiles (in cph) of $N^2(T, S)$ (line) and $N^2(T)$ (dash) along the equator for the (top) Pacific, (middle) Atlantic, and (bottom) Indian oceans (as shown in Figure 1).

where $N^2(T) > N^2(T, S)$ in the mean) occurs below the pycnocline in the Atlantic Ocean (0°N–35°W). More complex profiles are displayed in Figure 3 and exhibit structures like a double maxima in $N^2(T, S)$ (21°N–142°W (top left), 14°S–118°W (top right), and 15°S–35°W (middle right) or large differences for the depth of the maximum related to $N^2(T, S)$ and $N^2(T)$ such as occurs for 15°N–56°W (middle left). Consideration of the northern profile at 15°N–56°W shows a substantial signal in OSS that is typically representative of the Atlantic Ocean and that is almost nonexistent in the southern profile (15°S–35°W). In the Pacific subtropical gyres where the differences between maxima in $N^2(T)$, due to temperature alone, and $N^2(T, S)$, which characterizes the full density structure, are significant (Figure 3, top), the OSS is surprisingly weak and mainly confined in the upper layers. As discussed later, these signals exhibit strong seasonal variations in relation to the mixed layer and surface conditions and do not interfere with the main pycnocline located below the 200 m depth. In the Bay of Bengal (12°N–92°E, bottom left), we observe a remarkable stabilizing effect due to the salinity across the double maximum structure. Time series analysis at this position confirms that such an effect exists permanently throughout the year (not shown). To complete this broad overview, the profile at (23°S–114°W, bottom right) in the subtropical south Pacific reveals the case where the salinity structure never plays a stabilizing role throughout the upper 300 m depth of the water column.

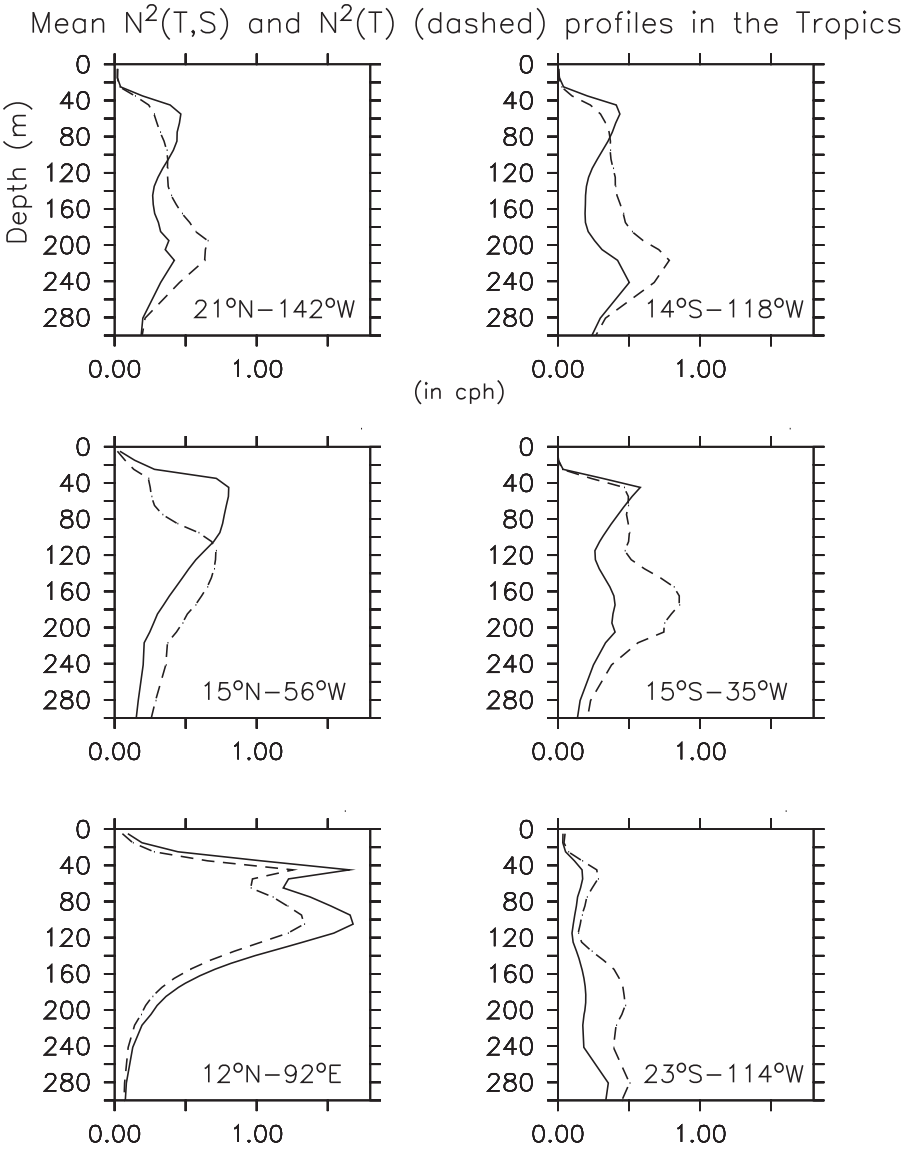

Figure 3. Annual mean profiles (in cph) of $N^2(T, S)$ (line) and $N^2(T)$ (dash) at different locations in the Tropics (as shown in Figure 1).

Figures 4 and 5 illustrate the spatial distribution of the seasonal OSS patterns, both in terms of amplitude and respective ratios of salinity to temperature contributions. In some regions, mainly localized within the subtropical gyres, the OSS as defined in this study does not exist and simply appears as the undefined regions in Figures 4 and 5.

These two figures clearly show the OSS to be a large-scale phenomenon characterizing the Tropics. Not surprisingly, the OSS in the region of the western Pacific Warm Pool is a permanent and substantial feature, roughly following the seasonal interhemispheric displacement of the warm (warmer than 28°C) and fresh (fresher than 34.8 psu) surface waters. In this region, the OSS effect explains 30–40% of the static stratification, a ratio that is quite stable at the seasonal time scale and slightly higher in the southern hemisphere, as compared to the northern one. Higher OSS values are found in the far eastern part of the Pacific basin, associated with the warm and fresh conditions of the far eastern Pacific fresh pool [*Alory et al*., 2012]. These seasonal variations could be also linked, to some extent, with the migrations of the Inter-Tropical Convergence Zone (ITCZ) across the entire Pacific basin. The signal is, however, confined in the main pycnocline that is close to the surface, and consequently does not explain on average more than 25% of the static stratification of the region (Figure 5). For some part, the above OSS signals in the Pacific are related to a freshening of the upper layers due to precipitation in regions where the SSS is characteristically lower than 34.8 psu.

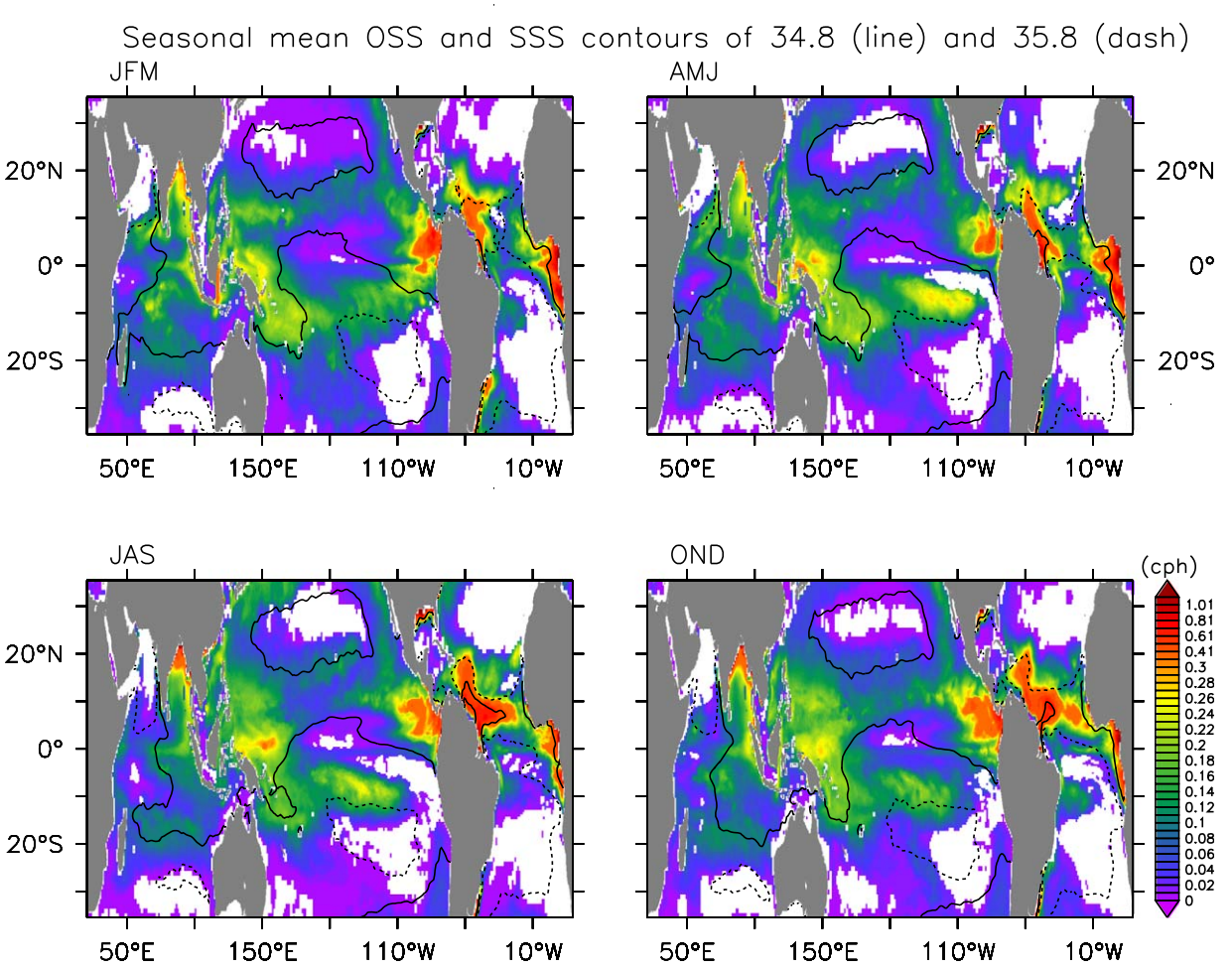

Figure 4. Seasonal maps of the ocean salinity stratification (OSS) (in cph) representing seasonal averages over January to March (JFM), April to June (AMJ), July to September (JAS), and October to December (OND). The black lines represent isolines for 34.8 (line) and 35.8 (dash) of the sea surface salinity.

The region of the central south Pacific exhibits a quite different behavior, with the presence of significant OSS in the boreal spring and summer accounting for more than 50% of the static stratification (the highest ratios are found in JAS). The absence of high and permanent precipitation in this region indicates that the processes involved in the formation and maintenance of OSS are quite different. As mentioned earlier, the mean profile in this region (Figure 3) shows the OSS occurring above the seasonal pycnocline in the upper 80 m depth. Figure 4 also reveals that this signal is confined in the region characterized by SSS between 34.8 and 35.8 psu.

Figure 6 shows a comparison between the seasonal profiles from the present analysis and direct and independent observations collected by two Argo floats in the same region in 2008. In temperature, the agreement is quite good, both in amplitude and in the shape of the profiles and the most important differences are located in the top layers with a warm bias for JAS and a cold bias for OND in the ocean reanalysis. The general form of the salinity profiles reveals that the OSS signal is due to the presence of fresh waters above typical salty conditions of the subtropical regions (i.e., salinity larger than 36.2 psu). This latter condition seems to be overestimated by the present reanalysis, while the differences both in temperature and salinity for JAS suggest that the mixing conditions are probably not strong enough. This point is to be the subject of further investigations as it could also relate to interannual variations and a lack of mixing. In any case, concurrent profiles of $N^2(T, S)$ show a quite good agreement in terms of their seasonal amplitude and the general forms along the water column. This comparison gives us some confidence on the accuracy of the OSS variability in this vast oceanic region of the south Pacific. As a quantitative measure of the degree to which the model deviates from the observations, and hence how well the model is constrained by the

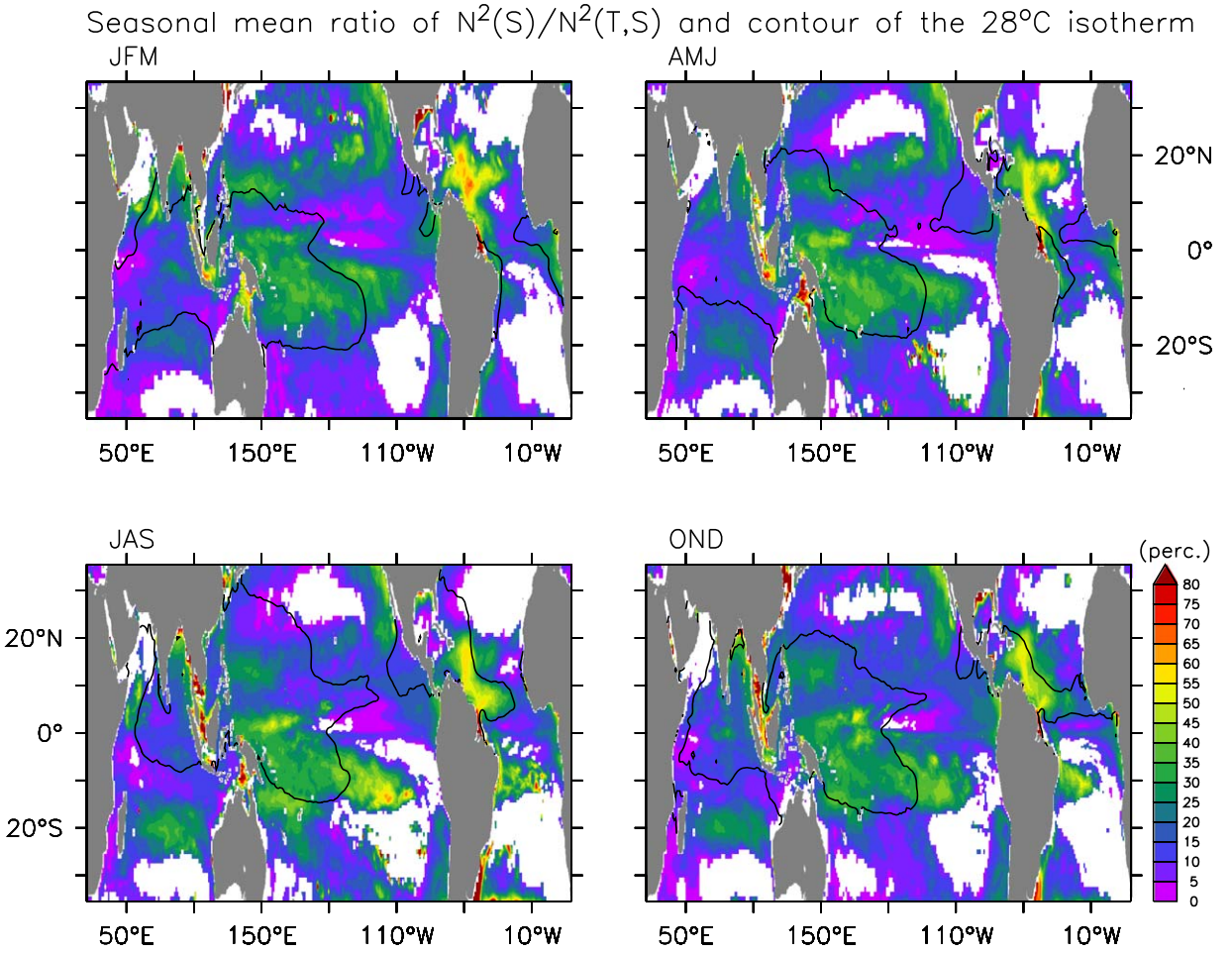

Figure 5. Seasonal maps of the ratio (in percentage) of $N^2(S)$ to $N^2(T, S)$. The thin black line marks the 28°C isotherm.

observations, we include the time evolution of the monthly mean background and analysis increments over the upper 1000 m for the Pacific averaged between 30°N and 30°S over the period 2001–2007 in supporting information (Figures S3).

In Figure 4, we identified significant regions in the Atlantic Ocean (between 0°N and 20°N and along the West African coast 10°S–10°N) having high OSS, particularly during the JAS and OND seasons. This region is characterized by important differences with regard to the Pacific that arise due to key components of the hydrological cycle including significant fresh-water discharges from several of the largest rivers of the world (e.g., Amazon, Orinoco, and Congo). Previous studies [e.g., *Hu et al.*, 2004] have shown that it is possible to track coherent regions of low surface salinity (generally less than 35 psu) over large distances offshore in the open ocean. These large-scale lenses of low salinity waters could now be monitored using SSS observations from space with the SMOS and Aquarius missions [*Lagerloef et al.*, 2008; *Reul et al.*, 2014]. The distribution of the seasonal OSS in the Atlantic Ocean (Figure 4) reveals that the largest amplitudes occur concurrently with significant variations of these large-scale lenses in the northwestern part of the basin and off the eastern coasts of Africa from the Gulf of Guinea southward of 8°S, i.e., near the mouth of the Congo river. The spatial extent of the OSS signal also suggests that the upper ocean circulation plays a major role as well as the other key fresh water source, namely the ITCZ.

In the North Atlantic Ocean, the maximum poleward extension of the OSS occurs in boreal winter (OND). The fact that the OSS dramatically decreases when the SSS becomes larger than 35.8 psu suggests that the vertical extension of the OSS signal is mainly confined in the upper layers of the ocean, typically above 100 m depth (see also the profiles of Figure 3). Relative to the thermal effect, the most important signal is associated with the extension of the fresh water from the Amazon, with the haline effect observed to become

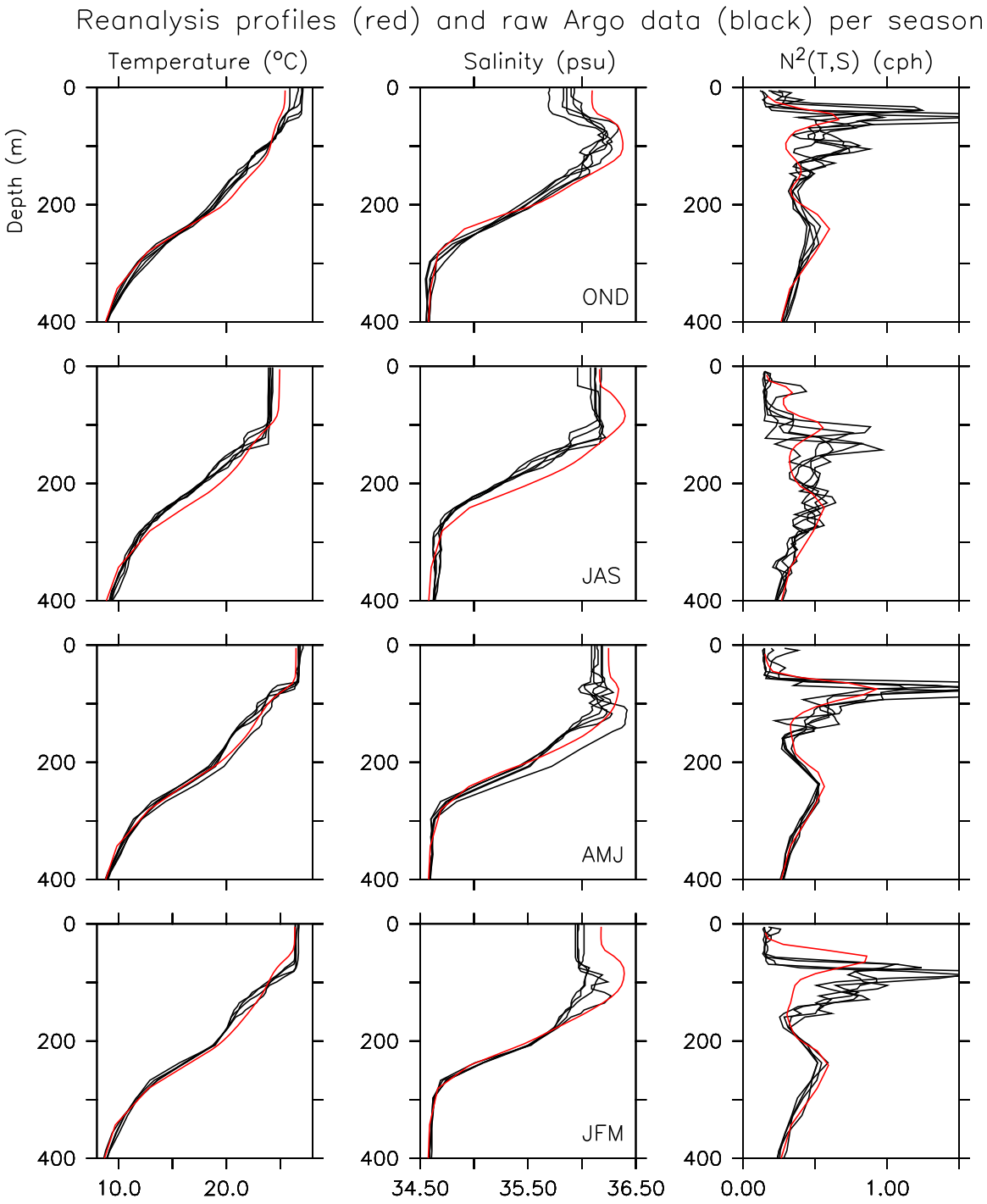

Figure 6. Independent vertical profiles of (left, in °C) temperature, (middle, in psu) salinity, and (right, in cph) N^2(T, S) collected by two Argo floats near 14°S–118°W in the tropical Pacific during 2008. The profiles are shown by season, following the JFM, AMJ, JAS, and OND periods, from bottom to top, respectively. On each panel, the average seasonal profile (2001–2007) at this location from the present reanalysis is shown in red.

dominant in the winter season (JFM) (Figure 5). It should be noted that the OSS exists also in the southwestern Atlantic Ocean near 10°S and it dominates the thermal effect during the boreal fall and winter season. In the Gulf of Guinea, the OSS exhibits large values but its ratio in comparison with the thermal effect remains modest throughout all the seasons (Figure 5). Being localized and close to the surface (see Figure 1) suggests that the OSS could have an indirect impact on SST (and on the mixed layer depth), and the coupling sensitivity of the Atlantic cold tongue, and consequently on the onset of the West African monsoon

[*Caniaux et al*., 2011]. Further work is needed to explore the full impact of the salinity stratification on the coupled response of the ocean-atmosphere variability.

In the North Indian Ocean, the zonal contrast between the Arabian Sea and the Bay of Bengal is evident and the OSS is almost absent in the former region. It should be nevertheless mentioned that significant amplitudes of OSS characterize the southeastern Arabian Sea during JFM-AMJ, a potential key region and timing that are crucial for the onset of the summer monsoon [*Masson et al*., 2005]. Across the whole basin, the strongest amplitudes in OSS are found along the coasts of the Bay of Bengal, with the maximum extension arising during the boreal summer and through the fall. Similar to the other tropical regions where precipitation is very intense, the signal is located in the upper layers; however, it represents only a modest contribution to the static stratification in comparison to the thermal effect over the same part of the water column (see Figure 5).

Along the equator, the specific wind regime associated with the monsoon system results in a complete reversal of direction at the seasonal time scale, with profound consequences for the current response down to the pycnocline. The equatorial variability of the OSS in the western Indian Ocean (Figure 4) exhibits a strong semiannual component with the highest values occurring at the end of March and September corresponding to the terminal periods of the winter and summer monsoons, respectively. Along the coast of Somalia, the variability is also very high with the most substantial OSS amplitudes occurring only from May to September where the maximum is reached in June near 45°E. In comparison to the thermal effect in the static stratification (Figure 5), the ratio of $N^2(T, S)$ to the salinity component $N^2(S)$ remains weak, in the range of 20–30%. The southern Indian Ocean between 10°S and 20°S differs substantially from the corresponding regions at the same latitudes of the Atlantic and Pacific Oceans. There, the OSS is permanently present across the whole basin with the variability characterized by a strong annual cycle. Here the OSS is dominant with typical ratios larger than 40% during JAS and lowest ratios occurring during the boreal winter JFM with typical basin averaged values less than 20% (Figure 5).

Finally, in order to complete the broad patterns of the OSS seasonal variability, a standard Fourier decomposition is used to describe the annual and semiannual cycles of the OSS field in the Tropics. Within the tropical band 20°N–20°S, the annual harmonics of the OSS dominates (Figure 7) with the largest values occurring in the Atlantic Ocean. Areas with a typical annual cycle larger than 0.1 cycles per hour (cph) in OSS include the western Pacific warm pool, the regions under the influence of the ITCZs, the southeastern Arabian Sea, and generally speaking the regions under the influence of the main river discharges into the ocean. In these regions, the fraction of explained variance of the annual harmonics is larger than 80% on average. The amplitude of the second harmonic (Figure 7b) is less than 0.1 cph over most of the ocean, with the largest areas of substantial amplitude found in the Atlantic, the eastern Pacific, and to a lesser degree the western north Indian Ocean. Values greater than 0.2 cph are found near the major river discharges into the ocean and in the Gulf of Panama, a feature that is shared with the semiannual cycle greater than 0.3 psu of the climatological SSS [*Boyer and Levitus*, 2002]. There are, however, two other regions of lesser amplitude where the semiannual cycle of the OSS appears to be important, namely the western equatorial parts of the Atlantic and Indian Oceans. In these regions, the percent of total variance attributed to the second harmonic exceeds 60% (Figure 7d). As noted earlier, such variability for the Indian Ocean may be associated with the semiannual occurrence of the monsoonal wind regime, and the one in the Atlantic sector with the semiannual cycle of the ITCZ over the South American continent. In the rest of the oceans, the general structure of the semiannual cycle appears less organized and patchy.

The basin-scale analyses presented above suggests that the seasonal variations of the global OSS are determined to first order by the atmospheric freshwater input and river runoff. Our concern is not to assess each mechanism in the formation and destruction of the OSS and we leave this for future investigations. The implied simple relationship between the OSS variations and the freshwater budget (P-E) is, however, more complex with closer examination, even in regions strongly influenced by precipitation such as under the South Pacific Convergence Zone and ITCZ. Figure 8 shows the seasonal variations of the OSS and (P-E) budget over three different regions of the northern hemisphere. The OSS variability exhibits a seasonal cycle with a maximum occurring at the end of summer, from September in the Atlantic Ocean to November in the Pacific Ocean. The relationships with the (P-E) budget show three different behaviors: in the Atlantic Ocean, both signals vary almost in phase (top). In the Bay of Bengal, the OSS amplitude responds with a delay, its maximum occurring at the end of the summer monsoon, in October (middle), while in the northern Pacific region under the ITCZ, the responses are clearly not in phase, the maximum of the OSS occurring

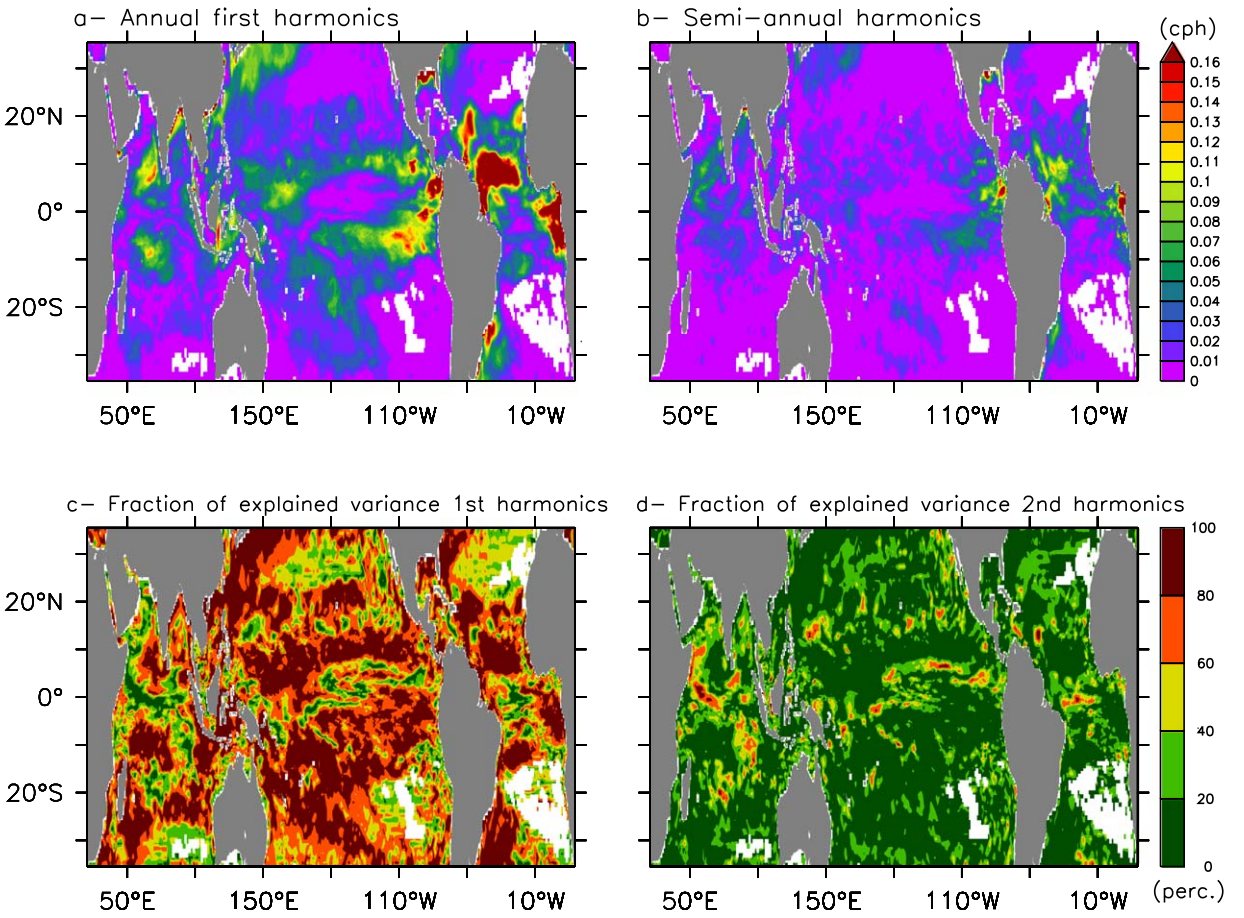

Figure 7. Maps of the (a) annual first and (b) semiannual second harmonics of the OSS (in cph), and of the fraction of explained variance for the (c) annual and (d) semiannual harmonics (in percentage).

in November, with a 3–4 months delay as compared to the maximum (P-E) budget (bottom). In contrast, both signals reach their minimum in March during the boreal spring. Previous studies elucidate the various and complex processes at work in the formation and destruction of the salinity stratification in the top-layers of the ocean [e.g., *Bosc et al.*, 2009]. The present study sheds light on the fact that these different processes would also apply from the surface down to the main pycnocline of the tropical oceans.

4. Discussion

Maes [2008] initially defined the OSS to better characterize the eastern edge of the Western Pacific Warm Pool (WPWP) where the haline stratification exhibits a permanent east-west gradient. The importance of such stratification in a region where the ocean and the atmosphere are tightly coupled and where these interactions would drive the ENSO variability has been previously revealed by the concept of the barrier layer. The recently available Aquarius and Argo data for salinity reveals the close relationship and variability of the barrier layer and WPWP displacements [*Qu et al.*, 2014]. Obviously, both the OSS and the BLT share some features in common, the main one being the representation of the stabilizing effect of the water column due to the salinity field. The shallow halocline that would mark the bottom of the upper mixed layer and the top of the thermocline has been named the barrier layer to highlight its role on the vertical turbulent mixing [e.g., *Lukas and Lindstrom*, 1991]. Inherently, the definition of the BLT is constrained by the need to fix appropriate thresholds and limits for the determination of the mixed layer depth and the top of the thermocline. Although the climatological BLT has been described on the global scale [*de Boyer Montégut et al.*, 2007], many studies dedicated to regional dynamics have redefined or adjusted their own determination of the BLT parameters. In contrast, we keep the idea of a single definition for the OSS as the part of the stabilizing effect due to salinity whatever the counterpart of the temperature effect could be. The OSS is

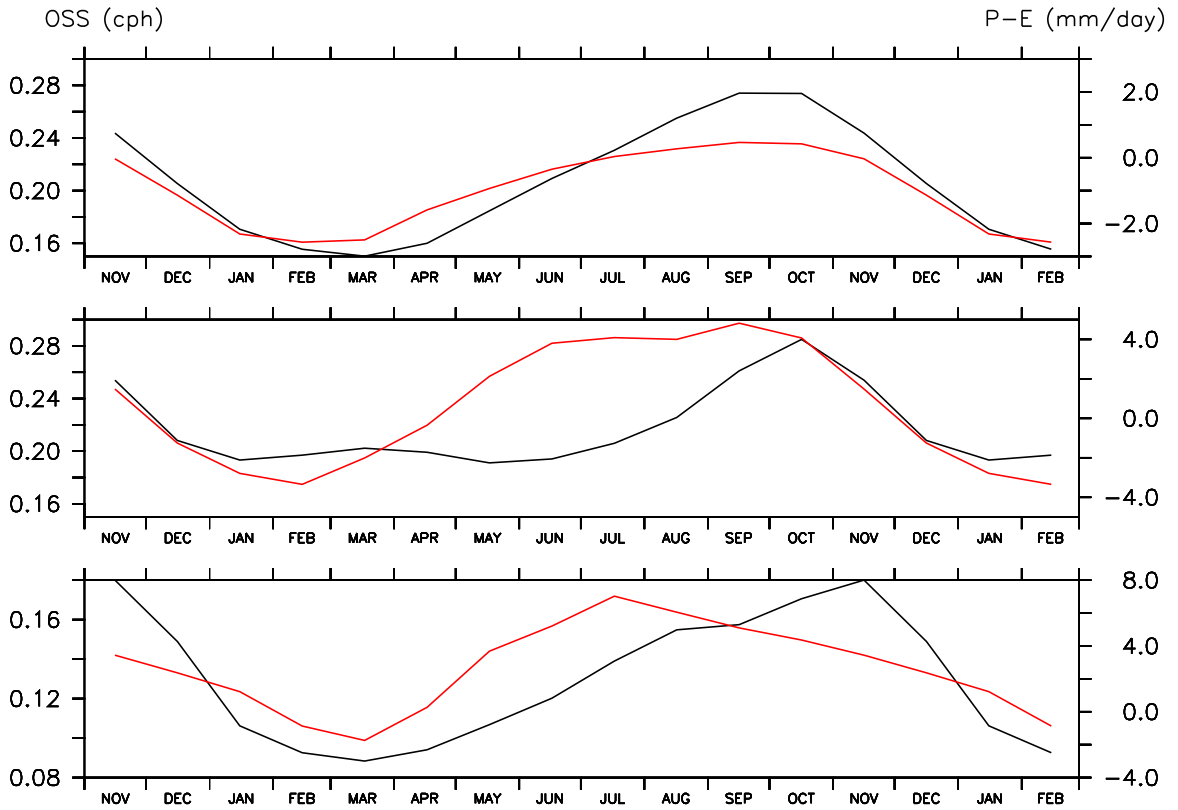

Figure 8. Seasonal variations of the OSS (left axis, in cph, black line) and P-E budget (right axis, in mm/day, red line) averaged over three different domains in (bottom, 5°N–15°N; 130°W–100°W) the Pacific Ocean, (middle, 5°N–25°N; 75°E–100°E) the Indian Ocean, and (top, 0°N–20°N; 290°E–340°E) the Atlantic Ocean.

defined from the definition of the Brunt Väisälä frequency profiles from which the dynamical properties, such as the first vertical baroclinic mode or internal Rossby radius of deformation, could be estimated. This approach includes very naturally the various parameterizations of vertical mixing that are Richardson-number dependent in numerical models.

In regions where the stratification of temperature and salinity differs between the base of the mixed layer and the top of the pycnocline, both the OSS and BLT agree relatively well; however, unlike the BLT the OSS can be significant in regions where both T and S are mixed over the same depth. In order to illustrate this difference, we examine the particular case of the western Pacific for the climatological month of July (Figure 9). Within the warmest waters of the equatorial warm pool (warmer than 29.5°C, dashed line), strong OSS signals illustrate the importance of the salinity stratification above the main thermocline. Differences appear not only in terms of the respective amplitudes of the OSS and BLT in the southern edge of the warm pool, but more importantly, the BLT does not exhibit significant values in regions like the far western Pacific or the Coral Sea. It is also immediately obvious that the region northward of 10°N from the dateline to the central Pacific is characterized by a clear signal in OSS, even where the SSTs are lower than 28°C. We will revisit the dependency of the OSS on the surface fields later.

In the far western Pacific as well as in the Coral Sea, the sections sampled in July by two independent cruises, respectively, the P09 WOCE and FLUSEC-01, show that significant vertical gradients in salinity result in OSS (Figure 10). For the first case, the salinity stratification occurs inside the waters warmer than 28°C and across the bottom of the mixed layer, resulting conjointly in significant BLT and OSS near the equatorial band; farther north (between 11°N and 19°N), there are also significant vertical gradients of salinity above 100 m depth that contribute to the amplitude of OSS below the mixed layer. The thermal gradient also plays a role in the static stratification of the water column, with a ratio of about 40–50% as compared to the salinity (computed similarly as in Figure 5 with the cruise profiles), consistent with the seasonal ratio reported previously in Figure 5 for the present reanalyses. For the second case, i.e., in the Coral Sea, the situation is a somewhat different. The salinity gradient in the eastern part of the section clearly occurs above

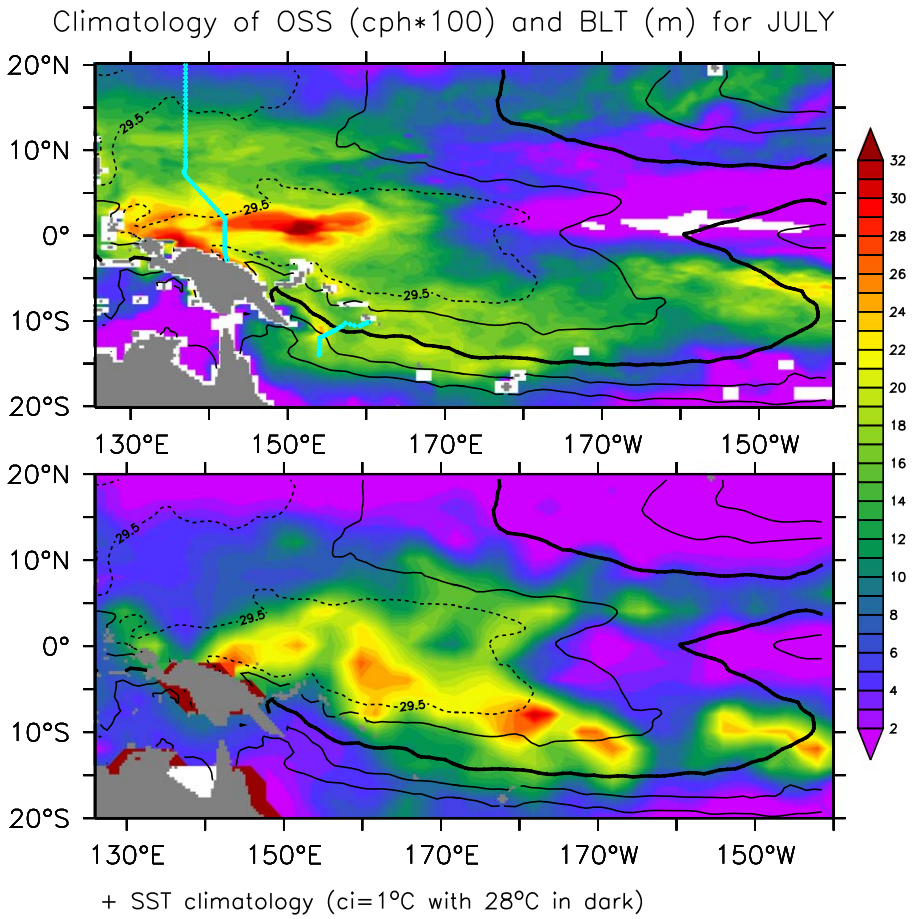

Figure 9. Maps of the (top) climatological OSS (in cph*100) and (bottom) climatological BLT (in m) for July. The BLT climatology is derived from *de Boyer Montégut et al.* [2007]. The climatological SSTs are superimposed in black, the dark and dash lines are set, respectively, for the 28°C and 29.5°C isotherms. On the top plot, the positions of the North Pacific and Solomon cruises are indicated by the light blue symbols.

the null gradient in temperature that is associated with the mixed layer. It should also appear in the climatological determination of the BLT. Whether the data coverage was not sufficient at the time of the realization of the BLT climatology or there is a subtle stratification in temperature that prevents the determination of the BLT as previously reported by *Maes* [2008] remains difficult to ascertain. In any case, it is clear that the salinity plays a significant part (>40%) in the static stratification of the waters of the Coral Sea that ultimately enter into the Solomon Sea from the surface throughout the thermocline [*Gasparin et al*., 2012]. How these waters are able to change the stratification along the equator is however beyond the scope of the present study and requires for future investigation.

The importance of the salinity stratification in the mixed layer of the Western Pacific Warm Pool was raised due to its potential impact on the mixed layer heat budget and SST, the key parameter in the ocean-atmospheric coupling. By removing the dependency of the salinity in N^2, *Maes et al*. [2002, 2005] and *Maes and Belamari* [2011] also demonstrated how different features of the ENSO variability and background mean state simulated by a coupled model could be fundamentally altered. Moreover, they found that the removal of the salinity stratification was not systematically associated with a cooling of the SST, and in a less important manner, with coherent changes in SSS. In the current Pacific climate, high SSTs represent a good proxy for positioning the deep atmospheric convection and their occurrence has also been associated with a thick barrier layer [i.e., *Bosc et al*., 2009]. In addition, *Maes* [2008] shows how the OSS was well correlated with the SSS near the equatorial WPWP. Owing to the availability of the SST and, more recently with the SMOS and Aquarius satellite missions for the SSS, the statistical relationships between the OSS and the surface fields could offer a way to evaluate the conditions of the main stratification above the pycnocline from a single parameter observed at the sea surface.

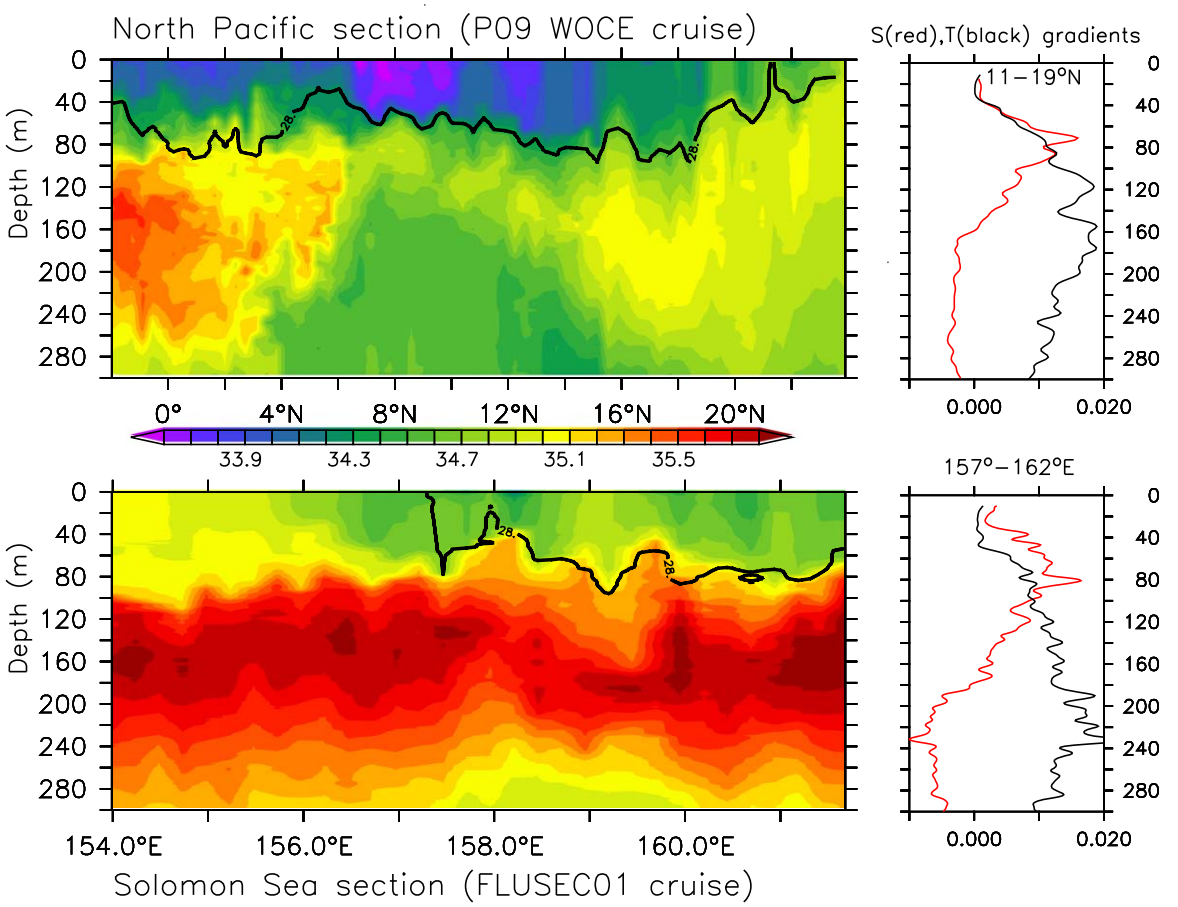

Figure 10. Vertical sections of salinity observed during (top) the P09 WOCE and (bottom) the FLUSEC-01 cruises. (right) the vertical gradient of salinity (unit is psu/m, in red) and temperature (unit in °C/m, in black and scaled by −0.2), respectively, for the positions between 11°N–19°N and 157°E–162°E. The thick line is the 28°C isotherm.

Figure 11 displays the scatter diagrams between the OSS and the surface fields of SST and SSS in three different regions of the Tropics. Consistent with *Maes* [2008], we find an inverse relationship between the OSS and SSS in the WPWP where large amplitudes of OSS are associated with the fresher waters, and then decreasing linearly as the SSS becomes saltier. In comparison, the relationship with the SST is less simple and obvious, with the exception that the higher SSTs (higher than 29.5°C) are often associated with significant OSS amplitudes. This result is consistent with those based on the barrier layer formalism as reported by *Fujii and Kamachi* [2003], *Bosc et al*. [2009], and *Fujii et al*. [2012]. Both in the Atlantic and the Indian Oceans, the relationship to the SST is more scattered and shows only a slight predominance of high OSS with high values of SST. In contrast, the relationship with the SSS exhibits smaller scatter and a quasilinear slope. In the Atlantic Ocean, there are fresh values that are not associated with a quasinull OSS amplitude and are located near the main river runoffs. The present scatter diagrams with the SSS field give some confidence that reliable observations of remotely sensed satellite missions for salinity would bring an additional source of information to better constrain the salinity stratification in the upper layers of the ocean. In certain regions where the dominant modes of variability in SSS exhibit their strongest amplitudes at the surface, like in the WPWP [i.e., *Maes*, 1999], the combination of different sources of observations would improve our understanding of the role of the salinity stratification in studies of the ocean dynamics.

5. Conclusions

In the present study, we examine seasonal variations of the OSS to emphasize its overall impact within the Tropics. Beyond its role at the base of the mixed layer, the stabilizing effect of salinity as depicted by the

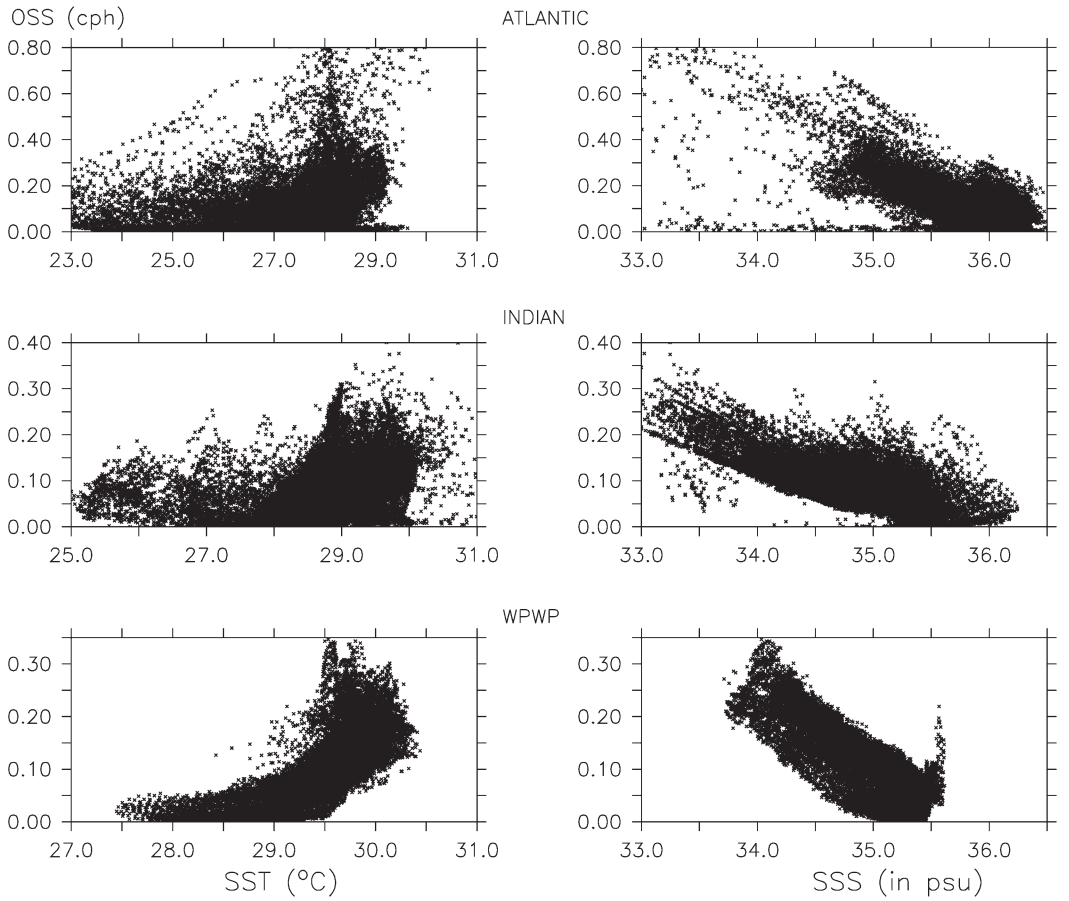

Figure 11. Scatter diagrams showing temperature (left, in °C) or salinity (right, in psu) against the OSS (in cph) in the 5°N–5°S equatorial band of the (top) Atlantic, (middle) Indian, and the Western Pacific Warm Pool as defined by the (bottom) 5°N–5°S/150°E–170°W box regions.

OSS has been shown to be seasonally important above the main pycnocline in many places in the tropical oceans. This includes regions not previously identified as important in terms of salinity stratification using the concept of the barrier layer (such as in the northwestern Pacific). The implication is that dedicated studies are now required in such places to determine the impact of the salinity stratification on the ocean dynamics. More generally, the formation of the OSS results from a complex combination of various mechanisms such as tropical precipitations, oceanic advection and mixing conditions, as well as fresh water input from rivers.

During the last decade, the key development of the ocean observing system has been the continued expansion of the Argo float network. Concomitant with temperature profiles, reliable in situ observations of salinity at depth are now available permanently at the global scales. Numerical systems developed for seasonal prediction and employing data assimilation could be utilized to investigate the impact of the salinity on climate variability. Recent results based on the state-of-the-art of prediction systems indicate that salinity is important for representing the state evolution of the equatorial thermocline [*Yang et al.*, 2010; *Zhao et al.*, 2013]. More recently, two satellite missions, the Soil Moisture and Ocean Salinity (SMOS) mission, which is part of the ESA's Earth Explorer Missions, and the Aquarius mission, which is a joint project of the United States and the Argentine SAC-D observatory, have begun to produce global maps of SSS [*Lagerloef et al.*, 2008; *Reul et al.*, 2014]. Reanalysis products that consider all these observations should be better able to produce accurate and reliable estimates of the salinity stratification above the main pycnocline and to offer new perspectives for a large spectrum of oceanographic studies. In that context, we hope that the present reanalyzed seasonal climatology of the ocean salinity stratification will provide an interesting step toward a better understanding of upper oceanic budgets and in validation of numerical ocean models.

Acknowledgments
The Argo data are collected and made freely available by the International Argo Project and the national programmes that contribute to it (http://www.argo.net). C. M. appreciates the support of an E. Frohlich Fellowship and thanks J. Brown for hosting his recent visit to CSIRO Marine and Atmospheric Research-Hobart in 2013. T. J. O. is funded by an Australian Research Council Future Fellowship and the Australian Climate Change Science Program. We would also like to thank the three anonymous reviewers for their comments on the original manuscript.

References

Alory, G., C. Maes, T. Delcroix, N. Reul, and S. Illig (2012), Seasonal dynamics of sea surface salinity off Panama: The far Eastern Pacific Fresh Pool, *J. Geophys. Res.*, *117*, C04028, doi:10.1029/2011JC007802.

Bloom, S. C., L. L. Takacs, A. M. da Silva, and D. Ledvina (1996), Data assimilation using incremental analysis updates, *Mon. Weather Rev.*, *124*, 1256–1271.

Bosc, C., T. Delcroix, and C. Maes (2009), Barrier layer variability in the western Pacific warm pool from 2000 to 2007, *J. Geophys. Res.*, *114*, C06023, doi:10.1029/2008JC005187.

Boyer, T. P., and S. Levitus (2002), Harmonic analysis of climatological sea surface salinity, *J. Geophys. Res.*, *107*(C12), 8006, doi:10.1029/2001JC000829.

Boyer, T. P., J. I. Antonov, H. Garcia, D. R. Johnson, R. A. Locarnini, A. V. Mishonov, M. T. Pitcher, O. K. Baranova, and I. Smolyar (2006), *World Ocean Database 2005*, chap. 1, NOAA Atlas NESDIS 60, edited by S. Levitus, 182 pp., U.S. Gov. Printing Off., Washington, D. C.

Caniaux, G., H. Giordani, J.-L. Redelsperger, F. Guichard, E. Key, and M. Wade (2011), Coupling between the Atlantic cold tongue and the West African monsoon in boreal spring and summer, *J. Geophys. Res.*, *116*, C04003, doi:10.1029/2010JC006570.

de Boyer Montégut, C., J. Mignot, A. Lazar, and S. Cravatte (2007), Control of salinity on the mixed layer depth in the world ocean: 1. General description, *J. Geophys. Res.*, *112*, C06011, doi:10.1029/2006JC003953.

Delworth, T., et al. (2006), GFDL's CM2 global coupled climate models Part 1: Formulation and simulation characteristics, *J. Clim.*, *19*, 643–674.

Fujii, Y., and M. Kamachi (2003), Three-dimensional analysis of temperature and salinity in the equatorial Pacific using a variational method with vertical coupled temperature-salinity empirical orthogonal function modes, *J. Geophys. Res.*, *108*(C9), 3297, doi:10.1029/2002JC001745.

Fujii, Y., M. Kamachi, S. Matsumoto, and S. Ishizaki (2012), Barrier layer and relevant variability of the salinity field in the equatorial Pacific estimated in an ocean reanalysis experiment, *Pure Appl. Geophys.*, *169*, 579–594, doi:10.1007/s00024-011-0387-y.

Gaspari, G., and S. Cohn (1999), Construction of correlation functions in two and three dimensions, *Q. J. R. Meteorol. Soc.*, *125*, 723–757.

Gasparin, F., A. Ganachaud, C. Maes, F. Marin, and G. Eldin (2012), Oceanic transports through the Solomon Sea: The bend of the New Guinea Coastal Undercurrent, *Geophys. Res. Lett.*, *39*, L15608, doi:10.1029/2012GL052575.

Griffies, S., et al. (2009), Coordinated ocean-ice reference experiments (COREs), *Ocean Modell.*, *26*, 1–46.

Gronell, A., and S. E. Wijffels (2008), A semiautomated approach for quality controlling large historical ocean temperature archives, *J. Atmos. Oceanic Technol.*, *25*, 990–1003.

Hu, C., E. T. Montgomery, R. W. Schmitt, and F. E. Muller-Karger (2004), The dispersal of the Amazon and Orinoco River water in the tropical Atlantic and Caribbean Sea: Observation from space and S-PALACE floats, *Deep Sea Res., Part II*, *51*, 1151–1171.

Kolodziejczyk, N., and F. Gaillard (2013), Variability of the heat and salt budget in the subtropical southeastern Pacific mixed layer between 2004 and 2010: Spice injection mechanism, *J. Phys. Oceanogr.*, *43*, 1880–1897.

Lagerloef, G., et al. (2008), The Aquarius/SAC-D Mission: Designed to meet the salinity remote-sensing challenge, *Oceanography*, *21*, 68–81.

Large, W., and S. Yeager (2009), The global climatology of an interannually varying air-sea flux data set, *Clim. Dyn.*, *33*, 341–364.

Lukas, R., and E. Lindstrom (1991), The mixed layer of the western equatorial Pacific Ocean, *J. Geophys. Res.*, *96*, 3343–3358.

Maes, C. (1999), A note on the vertical scales of temperature and salinity and their signature in dynamic height in the western Pacific Ocean: Implications for data assimilation, *J. Geophys. Res.*, *104*, 11,037–11,048.

Maes, C. (2008), On the ocean salinity stratification observed at the eastern edge of the equatorial Pacific warm pool, *J. Geophys. Res.*, *113*, C03027, doi:10.1029/2007JC004297.

Maes, C., and S. Belamari (2011), On the impact of salinity barrier layer on the Pacific Ocean mean state and ENSO, *SOLA*, *7*, 97–100.

Maes, C., J. Picaut, and S. Belamari (2002), Salinity barrier layer and onset of El Niño in a Pacific coupled model, *Geophys. Res. Lett.*, *29*(24), 2206, doi:10.1029/2002GL016029.

Maes, C., J. Picaut, and S. Belamari (2005), Importance of salinity barrier layer for the buildup of El Niño, *J. Clim.*, *18*, 104–118, doi:10.1175/JCLI-3214.1.

Masson, S., et al. (2005), Impact of barrier layer on winter-spring variability of the southeastern Arabian Sea, *Geophys. Res. Lett.*, *32*, L07703, doi:10.1029/2004GL021980.

McDougall, T. T. J. (1987), Neutral surfaces, *J. Phys. Oceanogr.*, *17*, 1950–1964.

O'Kane, T., R. Matear, M. Chamberlain, J. Risbey, B. Sloyan, and I. Horenko (2013a), Decadal variability in an OGCM Southern Ocean: Intrinsic modes, forced modes and metastable states, *Ocean Modell.*, *69*, 1–21.

O'Kane, T., R. Matear, M. Chamberlain, and P. R. Oke (2013b), ENSO and the late 1970's climate regime shift: The role of synoptic weather and South Pacific Ocean spiciness, *J. Comput. Phys.*, doi:10.1016/j.jcp.2013.10.058.

Oke, P., G. Brassington, D. Griffin, and A. Schiller (2008), The Bluelink Ocean Data Assimilation System (BODAS), *Ocean Modell.*, *21*, 46–70.

Oke, P. R., et al. (2013), Towards a dynamically balanced eddy-resolving ocean reanalysis: BRAN3, *Ocean Modell.*, *67*, 52–70, doi:10.1016/j.ocemod.2013.03.008.

Qu, T., Y. T. Song, and C. Maes (2014), Sea surface salinity and barrier layer variability in the equatorial Pacific as seen from Aquarius and Argo, *J. Geophys. Res. Oceans*, *119*, doi:10.1002/2013JC009375.

Reul, N., et al. (2014), Sea surface salinity observations from space with SMOS satellite: A new tool to better monitor the marine branch of the water cycle, *Surv. Geophys.*, in press, doi:10.1007/s10712-013-9244-0.

Sandery, P. A., G. B. Brassington, and J. Freeman (2011), Adaptive nonlinear dynamical initialization, *J. Geophys. Res.*, *116*, C01021, doi:10.1029/2010JC006260.

Sprintall, J., and M. Tomczak (1992), Evidence of the barrier layer in the surface layer of the tropics, *J. Geophys. Res.*, *97*, 7305–7316, doi:10.1029/92JC00407.

Thomson, R. E., and I. V. Fine (2003), Estimating mixed layer depth from oceanic profile data, *J. Atmos. Oceanic Technol.*, *20*, 319–329.

Yang, S.-C., M. Reinecker, and C. Keppenne (2010), The impact of ocean data assimilation on seasonal-to-interannual forecasts: A case study of the 2006 El Niño event, *J. Clim.*, *23*, 4080–4095.

Zhao, M., H. H. Hendon, O. Alves, Y. Yin, and D. Anderson (2013), Impact of salinity constraints on the simulated mean state and variability in a coupled seasonal forecast model, *Mon. Weather Rev.*, *141*, 388–402.